THE JOURNAL OF PHYSICAL CHEMISTRY A

ARTICLE

pubs.acs.org/JPCA

Reorientational Dynamics of the Dodecahydro-*closo*-dodecaborate Anion in $Cs_2B_{12}H_{12}$

Nina Verdal,*[,†] Terrence J. Udovic,[†] John J. Rush,[†,‡] Ronald L. Cappelletti,[†] and Wei Zhou[†,‡]

[†]NIST Center for Neutron Research, National Institute of Standards and Technology, Gaithersburg, Maryland 20899-6102, United States

[‡]Department of Materials Science and Engineering, University of Maryland, College Park, Maryland 20742-2115, United States

Supporting Information

ABSTRACT: Rapid reorientational motions of the $B_{12}H_{12}^{2-}$ icosahedral anion, a key intermediate in borohydride dehydrogenation, are revealed by quasielastic neutron scattering (QENS) measurements of $Cs_2B_{12}H_{12}$ between 430 and 530 K. At 430 K, over the range of momentum transfers collected, the elastic incoherent structure factor (EISF) is consistent with a model for reorientational jumps about a single molecular axis. At temperatures of 480 K and higher, however, the EISF suggests the emergence of multiaxis reorientation by dynamically similar, independent jumps about two axes, on average, preserving crystallographic order. Alternatively, if one assumes that the anions are undergoing temperature-dependent rotational trapping, then the EISF is also consistent with a jump model involving a temperature-dependent mobile fraction of anions statistically tumbling between discrete crystallographic sites. Although neutron vibrational spectra demonstrate that the anion torsional modes soften dramatically with increasing temperature, the QENS-derived activation energy of 333 meV for reorientation clearly shows that the anions are not undergoing isotropic rotational diffusion.

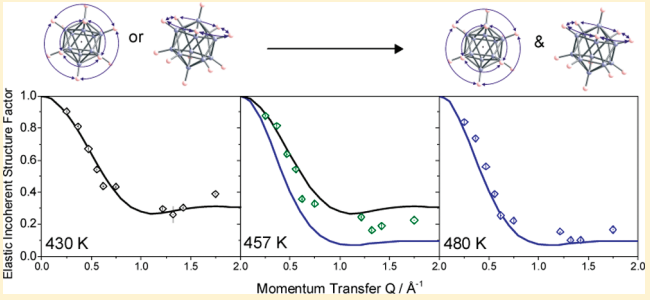

INTRODUCTION

Dicesium dodecahydro-*closo*-dodecaborate, $Cs_2B_{12}H_{12}$, is the heavy cousin of the lighter alkali-metal dodecahydro-*closo*-dodecaborates (e.g., $Li_2B_{12}H_{12}$ and $Na_2B_{12}H_{12}$), which have particular importance in current hydrogen-storage research, as they are known to be side-products in the dehydrogenation of the corresponding alkali-metal tetraborohydrides.[1] These compounds are ionically bonded salts comprised of alkali-metal cations and dodecahydro-*closo*-dodecaborate (i.e., $B_{12}H_{12}^{2-}$) icosahedral anions. Fundamental information concerning $B_{12}H_{12}^{2-}$ bonding potentials and dynamics, which are largely unknown, may provide valuable insights for understanding their stability and reactivity.

Recent ^{1}H and ^{11}B NMR spectroscopy results[2] suggest that the $B_{12}H_{12}^{2-}$ anions in the alkali-metal salts undergo rapid reorientational motions, with the motional frequency at a given temperature increasing as the cation radius and unit-cell dimensions increase. In order to explore the details of the anion motions, we investigated the dynamics of $B_{12}H_{12}^{2-}$ anions by neutron scattering techniques. To observe anion dynamics at reasonably low temperatures, we chose $Cs_2B_{12}H_{12}$, the salt with the largest alkali-metal cation (and hence the largest lattice constant). We probed both the $B_{12}H_{12}^{2-}$ reorientational dynamics by quasielastic neutron scattering (QENS) and the torsional and translational vibrational modes by neutron vibrational spectroscopy (NVS). In isolation, the $B_{12}H_{12}^{2-}$ anion is a regular icosahedron (depicted in Figure 1) but is susceptible to symmetry breaking by its environment.[3,4] $Cs_2B_{12}H_{12}$ crystallizes in the cubic space group $Fm\bar{3}$.[5] No phase transition was observed with DSC measurements[2] over the temperature range of 123−673 K.

EXPERIMENTAL METHODS

Isotopically labeled $Cs_2{}^{11}B_{12}H_{12}$ (>98% chemical purity, 99.5% isotopic purity) was purchased from Katchem.[6] The neutron absorption cross-section for ^{10}B is 7 orders of magnitude greater than that of ^{11}B, and the elimination of the ^{10}B isotope from the sample increases neutron transmission considerably. Prior to use, the material underwent vacuum dehydration at 300 °C for 4 h. The material was subsequently handled in a He-atmosphere glovebox. Data were collected from a polycrystalline powder that was contained in either an aluminum foil packet shaped into an annular geometry inside a cylindrical aluminum can or a steel foil packet inside a copper can. The approximate neutron transmission in both cases was 90%. The sample cans

Received: January 20, 2011
Revised: February 28, 2011
Published: March 17, 2011

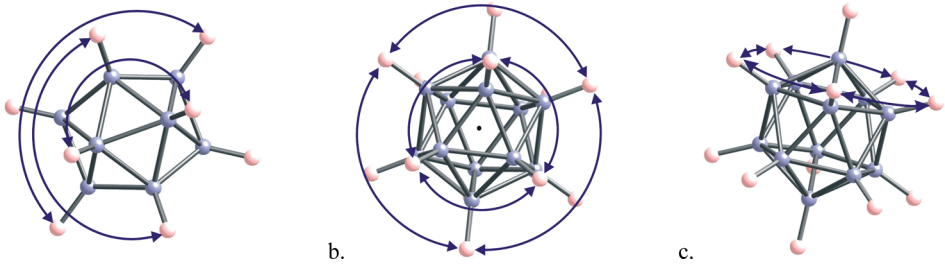

Figure 1. $B_{12}H_{12}^{2-}$ icosahedron. (a) Arrows depict hydrogen jumps about a C_2 rotational axis with jump distances of d_1 = 3.05 Å, d_2 = 4.93 Å, and d_3 = 5.80 Å. (b) Reorientational scheme for a C_3 rotation with two jump distances: d_1 = 3.05 Å and d_2 = 4.93 Å. (c) Depiction of reorientation about the C_5 axis, in which 10 hydrogen atoms jump, each over a distance of 3.05 Å, and two hydrogen atoms remain static.

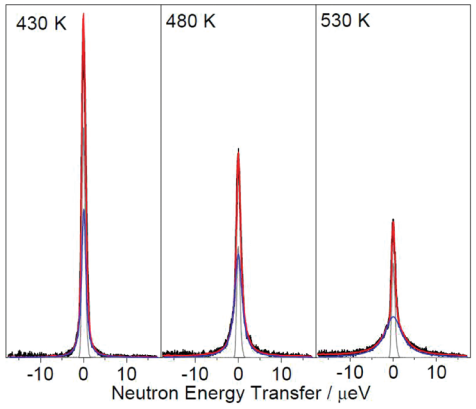

Figure 2. Quasielastic neutron scattering spectra (black) collected at 430, 480, and 530 K, shown with fitted functions (red lines) comprised of a resolution-limited elastic peak (gray), quasielastic Lorentzian peak (blue), and baseline. These particular spectra were observed at a momentum transfer of 0.62 $Å^{-1}$. The error bars representing $\pm 1\sigma$ are small and partly obscured by the plot traces.

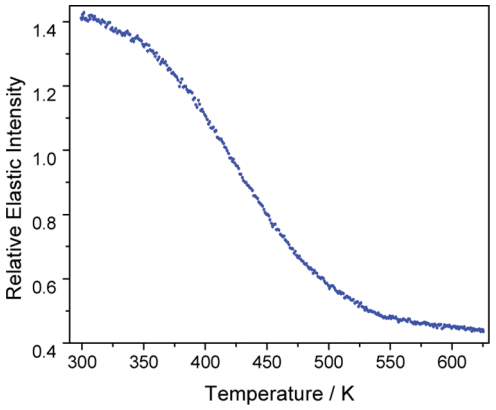

Figure 3. Fixed-window scan showing the elastic intensity as a function of temperature. Quasielastic spectra were collected between 430 and 530 K over the temperature range at which the elastic scattering loses intensity to the quasielastic scattering.

were sealed with either Pb or In gaskets and subsequently placed in a He closed-cycle refrigerator for neutron measurements.

All measurements were performed at the NIST Center for Neutron Research. The QENS measurements were performed on the High Flux Backscattering Spectrometer (HFBS)[7] with an incident neutron wavelength of 6.27 Å, momentum transfer (Q) over a range of 0.2−1.75 $Å^{-1}$, and a resolution of 0.83 μeV in most detectors. The quasielastic spectra were reduced and analyzed using the DAVE[8] software package. The vibrational density of states (VDOS) at 4 K was collected in neutron energy loss on the Filter Analyzer Spectrometer (FANS)[9] with a resolution of roughly 1 meV, and the VDOS at 100 K and higher were collected on the Disc Chopper Spectrometer (DCS)[10] with an instrument resolution between 0.4 and 1.2 meV over the energy range presented. The intensity of the vibrational peaks is determined by the mean-squared amplitude and the total neutron scattering cross section of the vibrating atoms.[11] Since hydrogen has a much larger cross section than other isotopes, vibrations with large hydrogen amplitude produce the most intense peaks.

First-principles calculations were performed within the plane-wave implementation of density functional theory (DFT) using the PWscf package.[12] Vanderbilt-type ultrasoft potentials were used with Perdew−Burke−Ernzerhof exchange correlation. A cutoff energy of 544 eV was found to be enough for the total energy to converge within 0.5 meV/atom. Structure optimizations were first performed with respect to atomic positions, with the lattice parameters fixed at the experimental values. Phonon calculations were then performed on the relaxed structures using the supercell method with finite displacements.[13]

RESULTS AND DISCUSSION

QENS probes hydrogen motion that occurs on the time scale of 10^{-8}−10^{-12} s. These motions are observed as μeV ($\sim 10^{-2}$ cm^{-1}) to meV (~ 8 cm^{-1}) changes in the energy of the neutron after collision with the molecular system. QENS spectra are composed of a strong elastic peak (a delta function convolved with a Gaussian-like instrument resolution function) and a broad quasielastic feature (usually fitted with a Lorentzian) that is a result of energy transfer (both loss and gain) between the neutron and the molecular system due to hydrogen motion. Examples of the QENS spectra collected for this system as a function of temperature are shown in Figure 2.

Temperatures at which the dynamics can be observed are found by collecting a fixed-window scan, a plot of the intensity of the elastic line as a function of temperature, shown in Figure 3. The intensity of the elastic line drops as arctangent as the quasielastic dynamics becomes broader than the instrument resolution and enters the quasielastic scattering window.[14] The fixed-window scan clearly shows that all rotational dynamics faster than 10^8 jumps/s is occurring well above 300 K. Quasielastic neutron scattering spectra were collected between 430 and 530 K, over the temperature range at which the elastic scattering

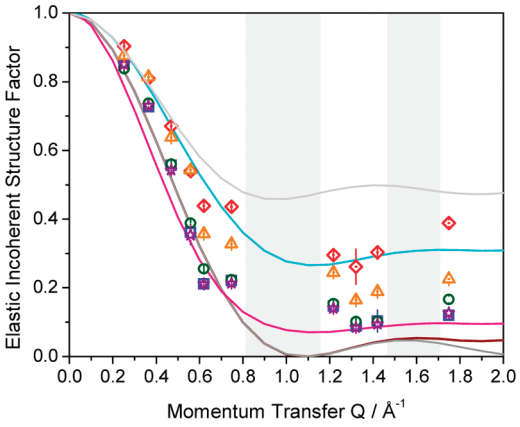

Figure 4. Observed EISF values for data collected at 530 (purple stars), 503 (blue squares), 480 (green circles), 457 (orange triangles), and 430 K (red diamonds) are compared with models for the reorientation mechanism: Jumps about a C_2 axis (light gray line), jumps about either a C_3 axis with two jump radii or jumps about a C_5 axis with the two axial hydrogen atoms static (cyan line), two-axis (C_5 and/or C_3) reorientations (pink line), discrete jumps about multiple axes (burgundy line), and isotropic rotational diffusion (dark gray line). The gray bands highlight the Q regions that are contaminated by Bragg peaks at 0.96, 1.1, and 1.58 Å^{-1}. The error bars may be smaller than the symbol and represent an uncertainty of one standard deviation.

loses intensity to the quasielastic scattering. The roughly linear decrease in elastic intensity as the temperature increases is due to the Debye−Waller factor.

The ratio of the intensity of the elastic and quasielastic scattering spectral features as a function of neutron momentum transfer (Q) can provide insight into the geometric mechanism of the rotational or translational motion. The Q-dependent, elastic incoherent structure factor (EISF) is the ratio of the elastic peak area $[A_0(Q)]$ to the sum of elastic and quasielastic $[A_1(Q)]$ peak areas

$$\mathrm{EISF} = \frac{A_0(Q)}{A_0(Q) + A_1(Q)} \tag{1}$$

in which $A_0(Q)$ and $A_1(Q)$ are related to the incoherent scattering function $S(Q,\omega)$ by[15,16]

$$S(Q,\omega) = A_0(Q)\delta(\omega) + A_1(Q)\frac{1}{\pi}\left(\frac{\frac{1}{\tau}}{\left(\frac{1}{\tau}\right)^2 + \omega^2}\right) \tag{2}$$

in a simple model in which the quasielastic contribution to the line shape can be represented by a single Lorentzian with a half-width at half-maximum (HWHM) of $(1/\tau)$. In practice, the observed features consist of $S(Q,\omega)$ convolved with the instrument resolution function and offset by a linear baseline.

The experimental EISF data between 430 and 530 K are shown in Figure 4. It should be noted that in this Q range the $Cs_2{}^{11}B_{12}H_{12}$ sample produces a strong Bragg peak (from coherent scattering) at 0.96 Å^{-1} and two weaker peaks at 1.12 and 1.58 Å^{-1}. This Bragg contamination manifests itself as increased elastic intensity at all temperatures in these Q regions [see Figure S1 in the Supporting Information]. These regions, designated by the vertical gray bands in Figure 4, are excluded from analysis. Figure 4 also depicts the calculated EISFs corresponding to a series of possible reorientation models for the $B_{12}H_{12}{}^{2-}$ icosahedral anion, ranging from discrete rotational jumps around a single axis, to discrete jumps about two axes, to discrete jumps around multiple axes resembling a tumbling motion, to isotropic rotational diffusion. If we ignore the crystal symmetry and focus on the local icosahedral symmetry of the $B_{12}H_{12}{}^{2-}$ anion, there are three types of symmetry axes to consider, C_2, C_3, and C_5, around which rotational jumps (of 180°, 120°, and 72°, respectively) leave the apparent orientation of the anion unchanged. Hence, the following models considered are (a) discrete reorientational jumps about one of the C_2 symmetry axes of the anion, (b) discrete reorientational jumps about one of the C_3 symmetry axes of the anion, (c) discrete reorientational jumps about one of the C_5 symmetry axes of the anion, (d) independent reorientational jumps around two axes, either C_3 or C_5, on the same time scale, (e) discrete jumps about multiple axes to any of the other hydrogen positions of the icosahedron, and (f) isotropic rotational diffusion.

For the C_2 discrete-jump model (a), the H atoms jump about a 2-fold (C_2) anion axis, preserving crystallographic symmetry. There are three types of H atoms, one of which jumps a short distance (d_1 = 3.05 Å) on a circle of smaller radius, one of which jumps a medium distance (d_2 = 4.93 Å) on a circle of intermediate radius, and one of which jumps a long distance (d_3 = 5.80 Å) on a circle of larger radius. This dynamic is illustrated in Figure 1a. The corresponding EISF

$$\mathrm{EISF}_{C_2}^{d_1,d_2,d_3} = \frac{1}{2}\left[1 + \frac{1}{3}j_0(Qd_1) + \frac{1}{3}j_0(Qd_2) + \frac{1}{3}j_0(Qd_3)\right] \tag{3}$$

where $j_0(x)$ is a zeroth-order spherical Bessel function equal to $\sin(x)/x$ and takes powder averaging into account. This model is based on 2-fold jump models developed elsewhere[15,17] and is represented in Figure 4 by the light gray line.

For the C_3 discrete-jump model (b), the H atoms jump about a 3-fold (C_3) anion axis, preserving crystallographic symmetry. There are two types of H atoms, one of which jumps a short distance (d_1 = 3.05 Å) on a circle of smaller radius and one of which jumps a medium distance (d_2 = 4.93 Å) on a circle of intermediate radius. This dynamic is illustrated in Figure 1b. The corresponding EISF

$$\mathrm{EISF}_{C_3}^{d_1,d_2} = \frac{1}{3}[1 + j_0(Qd_1) + j_0(Qd_2)] \tag{4}$$

is based on the 3-fold jump model developed elsewhere,[15,16] and a detailed derivation can be found in the Supporting Information. This model is represented in Figure 4 by the cyan line.

For the C_5 discrete-jump model (c), the H atoms jump about a 5-fold (C_5) anion axis, preserving crystallographic symmetry. Two out of 12 icosahedral hydrogen atoms define the 5-fold axis, remain stationary, and scatter only elastically. This dynamic is illustrated in Figure 1c. The corresponding EISF is actually identical to (and indistinguishable from) the EISF for the C_3 model with two jump distances (eq 4 and Figure 4). The derivation of this model is based on the formalism provided by Dianoux and co-workers[18,19] and can be found in the Supporting Information. The two H jump sites (d_1 = 3.05 Å and d_2 = 4.93 Å) in the C_5 model are the same as those in the C_3 model.

For the two-axis discrete-jump model (d), the two reorientational motions occur independently of one another and on the same time scale. In this case the quasielastic scattering function is

approximately represented by a convolution of the powder-averaged scattering functions $[S(Q,\omega)]$ of the individual motions about a C_5 and C_3 axis, two distinct C_3 axes, or two distinct C_5 axes

$$S(Q,\omega)_{\text{inc}}^{\text{obs}} = S(Q,\omega)_{\text{inc}}^{C_3} \otimes S(Q,\omega)_{\text{inc}}^{C_5} \quad (5)$$

Since the C_3 and C_5 models have identical EISFs, the resulting two-axis EISF is the same, no matter what type of axes are involved

$$\text{EISF}_{C_3 \otimes C_5} = \frac{1}{9}[1 + 2j_0(Qd_1) + 2j_0(Qd_2) + 2j_0(Qd_1)j_0(Qd_2) + j_0^2(Qd_1) + j_0^2(Qd_2)] \quad (6)$$

The derivation can be found in the Supporting Information. This function has a lower minimum than any of the single-axis functions.

The dynamics by which a proton jumps around multiple axes (e) to any of the other 11 discrete hydrogen positions at distances of d_1, d_2, and d_3 (in this case d_1 = 3.05 Å, d_2 = 4.93 Å, d_3 = 5.80 Å) on the icosahedron surface in an effective tumbling motion is described by the equation

$$\text{EISF}_{\text{icosahedron}} = \frac{1}{12}(1 + 5j_0(Qd_1) + 5j_0(Qd_2) + j_0(Qd_3)) \quad (7)$$

The individual terms are weighted by the probability that a site at that jump distance will be visited. This follows the formalism presented by Yildirim et al.[17] The minimum of this EISF represents a lower limit for all possible discrete-jump models.

In the isotropic rotational diffusion model (f), the H and B atoms remain covalently bound and the center of mass remains static but the rotating H atoms may be located anywhere on the surface of a sphere of radius r_0 = 2.9 Å, the distance between any H atom on the $B_{12}H_{12}^{2-}$ icosahedron and its center of mass. Thus, the anion rotates randomly in its position in the crystal lattice. The EISF is defined as[15,16]

$$\text{EISF}_{\text{iso}} = j_0^2(Qr_0) \quad (8)$$

This EISF is represented in Figure 4 by the dark gray line. The Q dependence of this dynamic differs from the discrete multiple-axis jump model only at high momentum transfers, which is apparent in Figure 4 by a comparison of the burgundy and dark gray lines.

It is evident from Figure 4 that the experimental EISF data deviate significantly from the isotropic rotational diffusion, multiple-axis discrete jump, and C_2 discrete-jump models. Rather, at 430 K, the lowest temperature measured, the observed EISF is in good agreement with the curve for either the single-axis C_3 or the single-axis C_5 model. As the temperature is increased to 457 K, the observed EISF starts to decrease toward the curve representing the two-axis jump model. At the highest temperatures of 480, 503, and 530 K, the observed EISFs have decreased further and now are in good agreement with the curve representing the two-axis jump model. Hence, within the accessible dynamic window of the spectrometer employed, there is a clear progression from single-axis reorientations at 430 K to two-axis reorientations by 530 K. Moreover, the data suggest that the temperature is not yet high enough to cause the anions to experience full multiple-axis tumbling or rotational diffusion.

Although the preceding models fit the temperature-dependent EISF, the notion of a preferred single axis or two axes of rotation may seem counterintuitive considering that there are multiple,

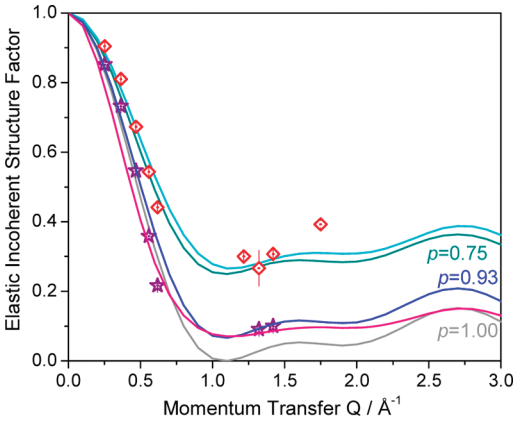

Figure 5. Observed EISF values for data collected at 430 (red diamonds) and 530 K (purple stars) are compared with models for jumps about either a C_3 axis with two jump radii or jumps about a C_5 axis with the two axial hydrogen atoms static (cyan line), two-axis (C_5 and/or C_3) reorientations (pink line), and multiple-axis discrete-jump tumbling (dark gray). Also shown are the multiple-axis tumbling model in which 1 out of 4 $B_{12}H_{12}^{2-}$ ions are in a trapped state (p = 0.75) and scatter only elastically (dark cyan) and the multiple-axis tumbling model in which one 1 of 15 $B_{12}H_{12}^{2-}$ ions are in a trapped state (p = 0.93) and scatter only elastically (dark blue line).

crystallographically identical C_2, C_3, and C_5 anion axes within the cubic lattice. Therefore, one might naturally assume that the anions would tend to perform multiple-axis jumps described above by the statistical tumbling model (e). Yet, such a model clearly is in disagreement with the data at all temperatures measured. Nonetheless, if one assumes that the anions undergo some type of temperature-dependent trapping that renders a fraction $(1 - p)$ of them rotationally immobile, then this will affect the height of the EISF. In this case, the protons from the immobile fraction would now only contribute to the elastic scattering intensity. If one assumes that only the mobile anion fraction (p) undergoes statistical tumbling, then the resulting EISF would be defined as

$$\text{EISF}_{\text{icosahedron}}^{\text{trapping}} = (1 - p) + p\left[\frac{1}{12}(1 + 5j_0(Qd_1) + 5j_0(Qd_2) + j_0(Qd_3))\right] \quad (9)$$

It is evident from Figure 5 that with the appropriate temperature-dependent value of p ($0.75 \leq p \leq 0.93$), eq 9 can describe the observed EISF over the temperature range measured. Thus, from the HFBS data alone, it is impossible to establish unequivocally the fine details of the reorientational mechanism. Indeed, the fact that the single-axis C_3 and C_5 models happen to fit the EISF so well at the lowest temperature cannot be easily dismissed as merely coincidental. However counterintuitive it may be, there is precedence in the literature[17,20] for single-axis and two-axis reorientational mechanisms. Low-temperature reorientations of NH_4Cl are found to occur about a single C_3 axis of the NH_4^+ cation, but in the high-temperature phase the reorientation is assigned to C_4 and C_3 jumps.[20] In the low-temperature ordered phase, cubane (C_8H_8) appears to reorient by a jump about a single 4-fold axis. In the disordered phase, the lower-temperature dynamic remains and is joined by a jump about a C_3 axis.[17] Such mechanisms are most likely driven by correlation effects from the neighboring lattice participants. It is clear from the magnitude of the reorientational barriers from simple first-principles calculations (which predict

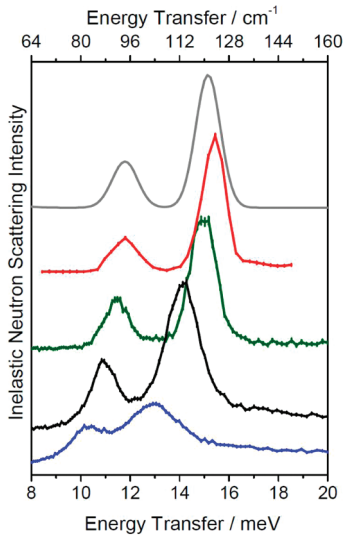

Figure 6. Low-energy VDOS of $Cs_2B_{12}H_{12}$ measured by neutron vibrational spectroscopy as a function of temperature. The spectra shown were collected (from bottom to top) in neutron energy gain at 550 (blue), 300 (black), and 100 K (green) and in neutron energy loss at 4 K (red). The feature at 11.8 meV (94 cm^{-1}) at 4 K is assigned as a translational mode and the peak at 15.4 meV (123 cm^{-1}) as a torsional mode. As the temperature increases, both peaks decrease in energy and broaden. The experiment is compared with the results of a 0 K periodic DFT calculation[4] (top, gray). The error bars representing $\pm 1\ \sigma$ are small and obscured by the plot traces. The spectra are vertically offset for ease of viewing.

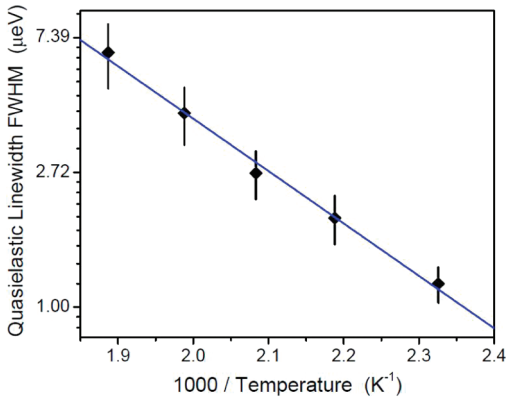

Figure 7. Arrhenius fit of the quasielastic line widths (full width at half-maximum (fwhm)) observed from 430 to 530 K. The fit yields an activation energy for reorientation of 32.3 ± 1.5 kJ/mol (333 ± 15 meV) and a pre-exponential factor $\tau_0 = (1.4 \pm 0.5) \times 10^{-13}$ s. The error bars represent one standard deviation and are calculated by propagating the error of the quasielastic line width.

overly large values ranging from 2.8 to 5.5 eV; see the Supporting Information) that the jump rotations of the $B_{12}H_{12}^{2-}$ anions (with an observed 333 meV barrier) must be a cooperative barrier-lowering reorientation involving neighboring anions and cations. It is not unreasonable to think that a single axis of rotation for a particular anion can persist for multiple jumps due to correlation effects before changing to another preferred axis. It is also not unreasonable to expect that such a single-axis mechanism will transform to a multiple-axis reorientation mechanism upon increasing the temperature.

As for the possibility of anion trapping, aside from the considerable presence of impurities or nonbulk-like grain boundary effects, it is not clear to us why any considerable fraction of the $B_{12}H_{12}^{2-}$ anions in the cubic lattice would become dynamically trapped. Granted, temperature-dependent hydrogen trapping has been known to occur[16,21] in solid-state systems with interstitial hydrogen and is attributed to hydrogen−hydrogen interactions within the lattice. Such trapping interactions immobilize a fraction of the site-hopping hydrogen, manifested clearly in the observed EISF. Yet, to the best of our knowledge, there are no good examples of reorientational trapping of otherwise crystallographically identical molecular species. Thus, we think that the argument is stronger for a rotational mechanism that does not involve trapping, i.e., the single-axis jump mechanism at 430 K that starts to become more multiple axis in character at 530 K.

In an effort to shed further light on the nature of the reorientation mechanism, we measured the low-energy vibrational density of states of $Cs_2B_{12}H_{12}$ from 8 to 20 meV (64 to 160 cm^{-1}). Figure 6 shows the VDOS measured at 4, 100, 300, and 550 K. The 11.8 and 15.4 meV features at 4 K have been assigned to the translational and torsional modes, respectively, in good agreement with the results of previous DFT calculations,[4] shown as the gray line in Figure 6. By 550 K, the translational and torsional modes have shifted roughly 1.6 and 2.4 meV lower in energy, respectively, both features broadening with temperature. At 4 K, the anion is primarily in its ground state, so the observed vibrational features reflect transitions from the ground-state to the first-excited-state energy levels. As the temperature is increased to 550 K, several higher translational and torsional energy levels become increasingly populated (*N.B.*, since kT at 12 K is equivalent to ∼1 meV, kT at 550 K ≈ 46 meV), and the spectra reflect contributions from a variety of transitions (i.e., 0 → 1, 1 → 2, 2 → 3, etc.), whose transition energies probably differ somewhat despite being identical in the harmonic case. Hence, these multiple transitions are at least partially responsible for the apparent softening and broadening at higher temperatures.

From our QENS data, the quasielastic line widths were fit to a single Lorentzian and plotted as a function of temperature. These data were fit with an Arrhenius function (Figure 7) yielding an activation energy for reorientation of 32.3 ± 1.5 kJ/mol (333 ± 15 meV ≈ kT at ∼3900 K) and a pre-exponential factor $\tau_0 = (1.4 \pm 0.5) \times 10^{-13}$ s. This activation energy is much higher than the observed torsion transition energy (15.4 meV) indicating that even at the elevated temperatures used in this study, the 3900 K barrier is still well above the populated excited-state torsional levels of the anions. Thus, the relatively high rotational barrier and the persistence of the torsional feature even at 550 K implies that there is still a bound oscillation deep within the well. Furthermore, one can conclude that any anion reorientation that occurs along the torsion coordinate experiences a large barrier to jump from near the bottom of one potential-energy well to the next. In short, the combined QENS and VDOS data strongly suggest that the icosahedral anions are reorienting via a jump mechanism rather than by isotropic rotational diffusion. Jumps occur over a barrier along the torsional mode coordinate to a minimum that is either a $2\pi/3$ or a $2\pi/5$ rotation (or a π rotation, if fully tumbling) from the previous configuration. Again, we are more inclined to think that rotational trapping in conjunction with statistical tumbling is not occurring. Rather, we propose that at 430 K rotational jumps occur predominantly about one molecular axis and between 480 and 530 K about two molecular axes on average.

Although the models for the C_3 and C_5 jump reorientation produce identical EISFs, the quasielastic contributions to the scattering are different for each model and in principle could be used to distinguish between them: the C_3 model requires only one Lorentzian to describe the quasielastic scattering, while the C_5 model requires two Lorentzians, one with a HWHM approximately 2.5× greater than the other (see Supporting Information). Even though a single Lorentzian provides a good fit to our observed data at 430 K, it does not eliminate the possibility of the C_5 reorientation. Fits to the quasielastic neutron spectra at 430 K using the parameters of either the C_3 or the C_5 model in which the τ is held constant over all Q are presented in Figure S4 of the Supporting Information. They produce similar χ^2 values and are inconclusive. In any case, the solid-state phonon calculation of the cubic structure predicts degenerate eigenvalues for the three torsional normal modes, and appropriate linear combinations of these eigenfunctions result in the same torsional energy about any rotational axis, including the C_3 and C_5 axes. Hence, at these high temperatures it is unclear a priori which axis is energetically preferred for reorientational jumps. Ultimately, sophisticated reaction path calculations would be necessary to determine the lowest energy reorientation pathway.

CONCLUSION

Over the temperature range investigated (430−530 K), the QENS and spectroscopic results suggest that the reorientation mechanism of the $B_{12}H_{12}^{2-}$ anions evolves from discrete jumps around one type of high-symmetry rotational axis (either C_3 or C_5) at the lowest temperature of 430 K to a combined mechanism involving, on average, independent (C_3 and/or C_5) two-axis discrete jumps between 480 and 530 K. Alternatively, the EISF is consistent with a jump model involving a temperature-dependent mobile fraction of anions statistically tumbling between discrete crystallographic sites. Ongoing work will investigate the dynamics of this anion over a larger range of temperatures and momentum transfers to further refine our understanding of the reorientation mechanism.

ASSOCIATED CONTENT

Supporting Information. Figure of the experimental EISF that includes all detectors, calculation for the potential barrier height along a one-dimensional torsion coordinate, QENS spectra fitted with C_3 and C_5 models, and derivations of the models used in the text. This material is available free of charge via the Internet at http://pubs.acs.org.

AUTHOR INFORMATION

Corresponding Author

*Phone: 301-975-6027. Fax: 301-921-9847. E-mail: nina.verdal@nist.gov.

ACKNOWLEDGMENT

This work utilized facilities supported in part by the National Science Foundation under Agreement No. DMR-0944772. This work was partially supported by the DOE through Award No. DE-AI-01-05EE11104 within the EERE-supported Metal Hydride Center of Excellence. The authors thank Dr. Timothy Jenkins for assistance with data collection on the HFBS spectrometer.

REFERENCES

(1) Hwang, S.-J.; Bowman, R. C.; Reiter, J. W.; Rijssenbeek, J.; Soloveichik, G. L.; Zhao, J.-C.; Kabbour, H.; Ahn, C. C. *J. Phys. Chem. C* **2008**, *112*, 3164–3169.

(2) Tiritiris, I.; Schleid, T.; Muller, K. *Appl. Magn. Reson.* **2007**, *32*, 459–481.

(3) Allis, D. G.; Hudson, B. S. *J. Phys. Chem. A* **2006**, *110*, 3744–3749.

(4) Verdal, N.; Zhou, W.; Stavila, V.; Her, J.-H.; Yousufuddin, M.; Yildirim, T.; Udovic, T. J. *J. Alloy Compd.* **2010**, in press; doi:10.1016/j.jallcom.2010.08.024

(5) Tiritiris, I.; Schleid, T. *Z. Anorg. Allg. Chem.* **2003**, *629* (7−8), 1390–1402.

(6) Identification of any commercial product or trade name does not imply endorsement or recommendation by the National Institute of Standards and Technology.

(7) Meyer, A.; Dimeo, R. M.; Gehring, P. M.; Neumann, D. A. *Rev. Sci. Instrum.* **2003**, *74*, 2759.

(8) Azuah, R.; Kneller, L.; Qiu, Y.; Tregenna-Piggott, P. L. W.; Brown, C.; Copley, J.; Dimeo, R. *J. Res. NIST* **2009**, *114* (6), 341–358.

(9) Udovic, T. J.; Brown, C. M.; Leão, J. B.; Brand, P. C.; Jiggetts, R. D.; Zeitoun, R.; Pierce, T. A.; Peral, I.; Copley, J. R. D.; Huang, Q.; Neumann, D. A.; Fields, R. J. *Nucl. Instrum. Methods A* **2008**, *588*, 406–413.

(10) Copley, J. R. D.; Cook, J. C. *Chem. Phys.* **2003**, *292*, 477.

(11) Squires, G. L. *Introduction to the Theory of Thermal Neutron Scattering*; Dover Publications: Mineola, NY, 1978.

(12) Giannozzi, P.; Baroni, S.; Bonini, N.; Calandra, M.; Car, R.; Cavazzoni, C.; Ceresoli, D.; Chiarotti, G. L.; Cococcioni, M.; Dabo, I.; Dal Corso, A.; Fabris, S.; Fratesi, G.; de Gironcoli, S.; Gebauer, R.; Gerstmann, U.; Gougoussis, C.; Kokalj, A.; Lazzeri, M.; Martin-Samos, L.; Marzari, N.; Mauri, F.; Mazzarello, R.; Paolini, S.; Pasquarello, A.; Paulatto, L.; Sbraccia, C.; Scandolo, S.; Sclauzero, G.; Seitsonen, A. P.; Smogunov, A.; Umari, P.; Wentzcovitch, R. M. *J. Phys.: Condens. Matter* **2009**, *21*, 395502.

(13) Kresse, G.; Furthmuller, J.; Hafner, J. *Europhys. Lett.* **1995**, *32*, 729.

(14) Prager, M.; Grimm, H.; Natkaniec, I.; Nowak, D.; Unruh, T. *J. Phys.: Condens. Matter* **2008**, *20*, 125218.

(15) Bée, M. *Quasielastic Neutron Scattering, Principles and Applications in Solid State Chemistry, Biology and Materials Science*; Adam Hilger: Bristol, 1988.

(16) Hempelmann, R. *Quasielastic Neutron Scattering and Solid State Diffusion*; Clarendon Press: Oxford, 2000.

(17) Yildirim, T.; Gehring, P. M.; Neumann, D. A.; Eaton, P. E.; Emrick, T. *Phys. Rev. B* **1999**, *60* (1), 314–321.

(18) Dianoux, A. J.; Volino, F.; Hervet, H. *Mol. Phys.* **1975**, *30* (4), 1181–1194.

(19) Sourisseau, C.; Lucazeau, G.; Dianoux, A. J.; Poinsignon, C. *Mol. Phys.* **1983**, *48* (2), 367–377.

(20) Töpler, J.; Richter, D. R.; Springer, T. *J. Chem. Phys.* **1978**, *69* (7), 3170–3181.

(21) Skripov, A. V.; Cook, J. C.; Udovic, T. J.; Kozhanov, V. N. *Phys. Rev. B* **2000**, *62* (21), 99–104.